Universities of Leeds, Sheffield and York
http://eprints.whiterose.ac.uk/

White Rose Research Online URL for this paper:
http://eprints.whiterose.ac.uk/83432

Published paper

CrossMark
click for updates

A non-invasive acoustical method to measure the mean roughness height of the free surface of a turbulent shallow water flow

A. Krynkin,[1] K. V. Horoshenkov,[1] A. Nichols,[1] and S. J. Tait[2]

[1]*Department of Mechanical Engineering, University of Sheffield, Mappin Street, Sheffield S1 3JD, United Kingdom*
[2]*Department of Civil and Structural Engineering, University of Sheffield, Mappin Street, Sheffield S1 3JD, United Kingdom*

In this paper, the directivity of the airborne sound field scattered by a dynamically rough free flow surface in a flume is used to determine the mean roughness height for six hydraulic conditions in which the uniform depth of the turbulent flow. The nonlinear curve fitting method is used to minimize the error between the predicted directivity and directivity data. The data fitting algorithm is based on the averaged solution for the scattered sound pressure as a function of angle which is derived through the Kirchhoff integral and its approximations. This solution takes into account the directivity of the acoustic source. For the adopted source and receiver geometry and acoustic frequency it is shown that the contribution from the stationary phase point (single specular point on the rough surface) yields similar results to those which can be obtained through the full Kirchhoff's integral. The accuracy in the inverted mean roughness height is comparable to that achieved with an array of conductive wave probes. This method enables non-invasive estimation of the flow Reynolds number and uniform flow depth. © 2014 Author(s). All article content, except where otherwise noted, is licensed under a Creative Commons Attribution 3.0 Unported License. [http://dx.doi.org/10.1063/1.4901932]

I. INTRODUCTION

Turbulent, shallow water flows form a common class of flow typical to gravel bed rivers, overland flows and drainage pipes. The surface of this type of flow is never flat and it is usually composed of complex patterns that are formed by the interaction of advecting turbulent structures with the free surface which represents the water-air interface. The dynamic pattern of this interface reflects the scale and frequency of the turbulent flow structures which cause the flow surface to appear rough.[1] The mean roughness height is one important characteristic of this roughness pattern which relates to the flow velocity and depth[2] and to the spatial frequency and scale of the turbulent structures which develop in this type of flow.[3] Given these relationships, accurate knowledge of this characteristic allows the possibility to estimate the key hydraulic parameters non-invasively by careful analysis of the free surface pattern.

There is a general lack or reliable airborne laboratory or *in situ* methods which can be used to measure characteristics of a dynamically rough free flow surface of a shallow water flow. Review of some existing methods for measuring the instantaneous water level elevation from air is given in Refs. 4 and 5. An alternative airborne acoustical method of roughness height measurement is proposed in this paper. This method is based on measuring the angular dependence of a harmonic acoustic wave scattered by the dynamically rough flow surface and fitting a mathematical model to the measured data. In this work, the dynamic surface roughness is assumed to be an ergodic process so that it is possible to use a sufficiently long time observation to deduce its statistical properties which are usually measured through a set of sufficiently large number of random realizations. This acoustical method is particu-larly attractive because the dynamically rough free surface is an acoustically rigid boundary so that it is relatively straight-forward to derive an exact mathematical formulation for the mean sound pressure in the acoustic wave scattered by this dynamic process.

There are two major approaches that can be used to predict the scattered acoustic field. These are: (i) the small perturbation method, where the acoustic wavelength $2\pi/k$ needs to be much longer than the mean roughness height σ (i.e., $k\sigma \ll 1$, k being the acoustic wavenumber in air) (see p. 72 in Ref. 6); and (ii) the Kirchhoff approximation where it is assumed that the sound wave incident on the rough surface undergoes only one specular reflection (see p. 183 in Ref. 6). In this paper, it is proposed to use the latter method. This is due to fact that the acoustic wavelength of the wave emitted by the source can be comparable to the mean roughness height, i.e., $k\sigma \sim 1$.

The Kirchhoff approximation for random surfaces is usually applied in the far field where $kR \gg 1$, e.g., in the Fraunhofer zone, where the ratio $k\sigma^2/R \ll 1$ and when $kL^2/R \ll 1$. Here R is taken as the distance between the source and specular reflection point and L is the characteristic dimension of the illuminated surface area. These assumptions allow the expansion of the integrand function in the Kirchhoff integral into a rapidly oscillating function. The stationary phase method is then applied so that the scattering cross section of the rough surface can be expressed in terms of its local curvature.[7] In some cases, there are more than one stationary phase point on the rough surface, which can contribute equally to the mean scattered sound pressure and intensity fields. In this case, it is possible to estimate the number of these specular points[8] and to identify the dynamics of these points[9] so that the

complexity of this process can still be captured without the need to evaluate explicitly the Kirchhoff integral.

In this paper, the illuminated area of the rough surface can be outside the Fraunhofer zone and the radial distance to the surface is comparable with the characteristic dimension of the illuminated patch. It is shown that for a given source and receiver geometry and Gaussian statistics of the rough surface process, one can estimate the mean sound pressure in the scattered field through the modified expression for the contribution from one specular reflection point taken on the equivalent smooth surface with which the rough surface can be replaced. This transformation enables the use of a relatively straightforward minimisation procedure to retrieve the mean roughness height from the measured angular dependence for the sound pressure above a dynamically rough water-air interface for a range of flow conditions.

In this paper, Sec. II describes the theoretical model and fitting functions which are based on the Kirchhoff integral and the single specular point approximation to it. In Sec. III, the experimental setup is detailed. This includes a description of the acoustic and hydraulic experiments and the data acquisition system which was used for data collection. The results of the inversion of the statistical parameters of the rough surface are discussed in Sec. IV.

II. THEORETICAL BASIS

Consider a rigid surface S which is dynamically perturbed around some equilibrium plane S_0 which coincides with the plane $z = 0$ as shown in Figure 1. The elevation of the surface is given by the homogeneous and stationary random field $z = \eta(\boldsymbol{r}, t)$ where $\boldsymbol{r} = (x, y, 0)$ is radius vector in Cartesian coordinates and t is the time. This surface represents the dynamically rough water-air interface of a turbulent shallow water flow. Assuming that the given random field is an ergodic process[10] with respect to time, the statistical properties of a single, sufficiently long realisation of this field $z = \eta(\boldsymbol{r}, t)$ are representative of the statistical properties of an infinite number of realizations of the random field $z = \eta(\boldsymbol{r})$. It is also assumed that the distribution of the random field $z = \eta(\boldsymbol{r})$ obeys the Gaussian probability density function $w(\eta, \boldsymbol{r})$
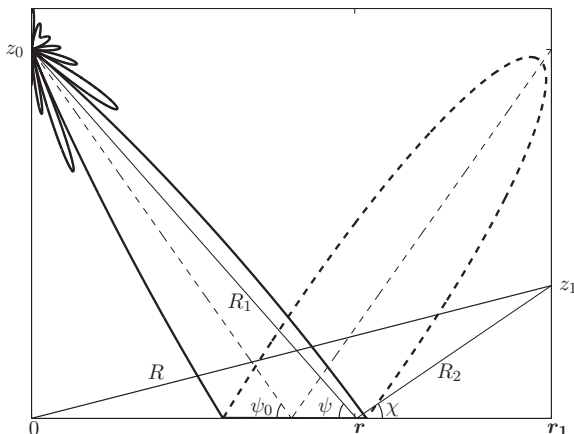

FIG. 1. Geometry of the problem.

with

$$\overline{\eta(\boldsymbol{r})} = 0, \tag{1}$$

$$\overline{\eta(\boldsymbol{r})\eta(\boldsymbol{r})} = \sigma^2. \tag{2}$$

In Eqs. (1) and (2) operation $\overline{\langle\cdot\rangle}$ stands for averaging over all possible realisations for the pattern of $\eta(\boldsymbol{r})$ which one can observe over a representative period of time so that

$$\overline{\eta(\boldsymbol{r})} = \int\limits_{-\infty}^{+\infty} \eta(\boldsymbol{r})w(\eta, \boldsymbol{r})\mathrm{d}\eta, \tag{3}$$

where the probability density function is given by

$$w(\eta, \boldsymbol{r}) = \frac{1}{\sigma\sqrt{2\pi}} \exp\left(-\frac{\eta^2}{2\sigma^2}\right). \tag{4}$$

In this paper, the acoustic source and receiver are located above the surface at points $(0, 0, z_0)$ and $(x_1, 0, z_1)$, respectively (see Figure 1). It is assumed that scattering of acoustic waves from the given random rigid surface can be approximated by the reflection from a tangential plane at each point $\boldsymbol{r} = (x, y)$ of this surface (Kirchhoff approximation). To satisfy the Kirchhoff approximation it is required that[6]

$$(hk)^{1/3} \sin(\psi) \gg 1, \tag{5}$$

where h is the characteristic radius of curvature of $\eta(\boldsymbol{r})$, ψ is the angle of incidence, and $k = \omega/c$ is the wavenumber defined through the angular frequency ω and speed of sound c.

It is also assumed that the acoustic source is a point source which is directional, and that its directivity in the far field is given by

$$A(\phi) = \mathcal{A}\frac{J_1(ka\sin\phi)}{ka\sin\phi}, \tag{6}$$

where a is radius of the circular aperture, ϕ is the zenith angle in spherical coordinates (r, θ, ϕ), and $\mathcal{A}$ is the amplitude of the source.[11]

The main axis of the directed source is in the Oxz plane (see Figure 1) and it is inclined at angle ψ_0 to the Ox axis and $\pi/2 - \psi_0$ to the Oz axis. Therefore, the angle ϕ is defined by

$$\phi = \arccos\left(\frac{z_0}{R_1}\right) - \left(\frac{\pi}{2} - \psi_0\right), \tag{7}$$

where $R_1 = \sqrt{x^2 + y^2 + [z_0 - \eta(x, y)]^2}$ is distance to the surface S from the source at a fixed point $(x, y, \eta(x, y))$. It is noted that throughout this paper R_1 will be taken as the distance from the source to the smooth surface S_0.

The characteristic dimension of the illuminated area of the rough surface L is assumed to be comparable with the distance R_1, i.e.,

$$L \sim R_1. \tag{8}$$

A. Mean value of the scattered sound field

In the far-field where the distances from the source and receiver to a fixed point on the rough surface are much greater than the acoustic wavelength, the scattered acoustic

field above the rough surface S can be approximated by the Kirchhoff integral which is taken over the illuminated smooth surface S_0, i.e.,[6]

$$p_s(\boldsymbol{R}) \approx \frac{1}{4\pi i} \int_{S_0} V A(\phi) \boldsymbol{n}\boldsymbol{q} \frac{e^{i[k(R_1+R_2)-q_z\eta(r)]}}{R_1 R_2} \frac{d\boldsymbol{r}}{n_z}, \qquad (9)$$

$$\boldsymbol{n} = \frac{e_z - \boldsymbol{\gamma}(\boldsymbol{r})}{\sqrt{1 + \boldsymbol{\gamma}(\boldsymbol{r})^2}}, \qquad (10)$$

$$\boldsymbol{q} = -k\nabla(R_1 + R_2), \qquad (11)$$

$$\boldsymbol{\gamma}(\boldsymbol{r}) = \nabla_r \eta(\boldsymbol{r}), \qquad (12)$$

where $\boldsymbol{R}$ is the radius vector pointed at the receiver, e_z is the component of a unit vector $\boldsymbol{n}$ normal to the rough surface S at the fixed point $\boldsymbol{r} = (x, y, 0)$. $R_1 = \sqrt{x^2 + y^2 + z_0^2}$ and $R_2 = \sqrt{(x_1 - x)^2 + y^2 + z_1^2}$ are distances to surface S_0 at fixed point $\boldsymbol{r}$ from the source and receiver, respectively. Because it is assumed that surface S is rigid, the reflection coefficient in the Kirchhoff approximation is set to $V = 1$.

The far-field conditions can be represented as $kR_1 \gg 1$ and $kR_2 \gg 1$, indicating that the acoustic wavelength is much smaller than the distance to the surface. Assuming that distances R_1 and R_2 are of the same magnitude compared to the acoustic wavelength, then the far-field conditions can be defined as

$$kR \gg 1, \qquad (13)$$

where R is referred to as the characteristic distance to the reflecting surface as shown in Figure 1.

It is noted that to derive Eq. (9) the source and receiver should be in the Fraunhofer zone with respect to the elevated point on the surface S so that

$$\frac{k\sigma^2}{R} \ll 1. \qquad (14)$$

However, due to the condition (8), the far-field assumption (13) leads to the conclusion that within the illuminated area of the rough surface a multiple number of Fresnel zones can be observed, i.e.,

$$\frac{kL^2}{R} \gg 1. \qquad (15)$$

This prevents the use of those approximations which only work in the Fraunhofer zone (see p. 229 in Ref. 6).

Expanding the scalar product $\boldsymbol{n}\boldsymbol{q}$ in Eq. (9) the scattered acoustic pressure appears as

$$p_s(\boldsymbol{R}) = \frac{1}{4\pi i} \int_{S_0} A(\phi) \frac{e^{ik[R_1+R_2-q_z\eta(r)/k]}}{R_1 R_2} q_z \left[1 - \frac{\boldsymbol{q}\boldsymbol{\gamma}(\boldsymbol{r})}{q_z}\right] d\boldsymbol{r}, \qquad (16)$$

where $q_z = k(z_0/R_1 + z_1/R_2)$.

In order to simplify the problem, the shadowing effects on the rough reflecting surface can be neglected, which gives

$$\frac{\boldsymbol{q}\boldsymbol{\gamma}(\boldsymbol{r})}{q_z} \ll 1. \qquad (17)$$

In the case of a one-dimensional rough surface, i.e., when the roughness function depends only on one coordinate, $\eta = \eta(x)$,

condition (17) for the forward scattering can be transformed into

$$|\gamma| \ll \cot\left(\frac{\psi - \chi}{2}\right). \qquad (18)$$

The mean scattered acoustic pressure can be found by applying averaging (3) to Eq. (16). This gives

$$\overline{p_s(\boldsymbol{R})} = \frac{1}{4\pi i} \int_{S_0} A(\phi) \frac{e^{ik(R_1+R_2)}}{R_1 R_2} q_z e^{-\sigma^2 q_z^2/2} d\boldsymbol{r}. \qquad (19)$$

The explicit parametric dependence of the mean sound pressure on the mean roughness height can be exploited to measure the latter by minimising the difference between the model and the measured data. This procedure is discussed in Sec. III. The unique solution of this minimisation problem is ensured by monotonic behaviour of the mean sound pressure (19) as a function of the mean roughness height.

B. Method of stationary phase

The solution of Eq. (19) can be found through the numerical integration which can be performed with the quadrature rule. However, it is proposed to use the stationary phase method[12] which is suitable when conditions (13) and (15) are satisfied. This method enables avoidance of the numerical integration procedure which is problematic when the integrand function in Eq. (16) is rapidly oscillating. According to this method the value of the integral in Eq. (16) can be approximated with the sound pressure in the wave reflected by the rough surface at the specular reflection point $\boldsymbol{r}_s$ for which

$$\nabla_r \alpha(\boldsymbol{r}) = \nabla_r [R_1 + R_2 - q_z\eta(\boldsymbol{r})/k] = 0 \quad \text{and} \quad \boldsymbol{r}_s \in S_0. \qquad (20)$$

In this work, it is assumed that some realisations of the rough surface S may contain multiple stationary phase points M. In this case, the integral in (16) can be expanded as

$$p_s(\boldsymbol{R}) \approx \frac{1}{2ik} \sum_{m=1}^{M} \frac{f(r_{sm}) e^{ik\alpha(r_{sm})+i\beta_m\pi/4}}{\sqrt{|D(r_{sm})|}}, \qquad (21)$$

where

$$f(r_{sm}) = \left[\frac{A(\phi)q_z}{R_1 R_2}\right]_{r=r_{sm}}, \qquad (22)$$

$$\alpha(r_{sm}) = [R_1 + R_2 - q_z\eta(\boldsymbol{r})/k]_{r=r_{sm}}, \qquad (23)$$

$$D(r_{sm}) = \left[\frac{\partial^2\alpha}{\partial x^2}\frac{\partial^2\alpha}{\partial y^2} - \left(\frac{\partial^2\alpha}{\partial x\partial y}\right)^2\right]_{r=r_{sm}}, \qquad (24)$$

and

$$\beta_m = \begin{cases} 2 & \text{if } \operatorname{sgn}\left(\frac{\partial^2\alpha}{\partial x^2}\right) > 0, \ \operatorname{sgn}(D) > 0, \\ 0 & \text{if } \operatorname{sgn}(D) < 0, \\ -2 & \text{if } \operatorname{sgn}\left(\frac{\partial^2\alpha}{\partial x^2}\right) < 0, \ \operatorname{sgn}(D) > 0. \end{cases} \qquad (25)$$

In this paper, the interval of the random realizations of rough surface $\eta(\boldsymbol{r})$ where the specular point is observed corresponds

to the concave surface (23). The presence of the relatively large terms, R_1 and R_2 in the phase function $\alpha(\mathbf{r})$ makes its second partial derivative with respect to x as well as Gaussian curvature $1/D$ positive which ensures that the surface is concave. This enables us to assume that $\beta = 2$.

The above approach is based on the principle similar to that outlined in Bass and Fuks (see p. 252 of Ref. [6]) which can be used to derive the mean intensity of the scattered acoustic field in the Fraunhofer zone, and in Kodis[7] which can be used to derive the equivalent cross-section for scattering of electromagnetic waves by a rough surface provided that condition (5) is satisfied. Equation (21) derived in this paper is an extension of the approach proposed in Refs. [6] and [7], because it enables the integral to be estimated when the Fraunhofer zone approximation is no longer satisfied.

In the far field (Fraunhofer zone) and mirror direction with respect to the main axis of the directed source ($\chi_0 = \pi - \psi_0$), Barrick[13](Eq. (8)) showed that for an isotropically rough surface (i.e., a surface for which the correlation radius l for the surface roughness pattern is independent from direction) the number of specular points M within the square with length l can be estimated from

$$M l^2 \approx 1. \tag{26}$$

This number shows that in the vicinity of the angle χ_0 and within the random rough surface correlation length the number of specular points tends to one. It is also noted that estimation of the number of specular points in Eq. (26) is independent from σ and, therefore, can be applied to surfaces with arbitrary mean roughness height.

The relationship (26) indicates that if the correlation length is comparable with the characteristic size of the illuminated area the sum in Eq. (21) can be truncated to a single term which is defined by the reflection from the specular point on the equivalent smooth surface S_0, i.e.,

$$\mathbf{r}_{sm} = \left(\frac{x_1 z_0}{z_0 + z_1}, 0, 0 \right). \tag{27}$$

It is also possible to simplify Eq. (20) to justify the choice of a single specular point for at least the mirror angle χ_0 case. If the source and receiver have the same distance to the rough surface (i.e., $z_0 = z_1$) and the receiver is positioned on the line of specular reflection with angle χ_0 from the smooth surface S_0 (i.e., $R = R_1 = R_2$), then the gradient of the phase (20) will give the following approximate coordinates of the specular point:

$$\begin{aligned} x &\approx \frac{x_1}{2} + z_0 \gamma_x, \\ y &\approx z_0 \gamma_y, \end{aligned} \tag{28}$$

where γ_x and γ_y are the components of the slope defined in Eq. (12) and their orders are given by Eq. (17). In these equations for specular point coordinates (28), the items containing $\eta(\mathbf{r})/R$ term are neglected as they are insignificant. It can now be seen that coordinates x and y in Eq. (28) can take values different from the specular point of the smooth surface if the source and receiver are elevated from the surface at a distance much higher than that used in this paper so that $z_0 |\boldsymbol{\gamma}| = \mathcal{O}(1)$.

In order to determine the mean sound pressure it is necessary to apply the averaging procedure according to Eq. (3) in which the probability density function is given by Eq. (4). This yields

$$\overline{p_s(\mathbf{R})} \approx \frac{1}{2k} \frac{f(\mathbf{r}_s)}{\sqrt{|D(\mathbf{r}_s)|}} e^{ik(R_1 + R_2) - \sigma^2 q_z^2 / 2}. \tag{29}$$

Equations (19) or (29) can be used to predict the directivity of the mean sound pressure field scattered by the dynamically rough surface. These predictions will be compared against the experimental data in Sec. IV.

III. EXPERIMENTAL PROCEDURES

A. Hydraulic setup

In order to study the validity of the theoretical model proposed in Sec. II, a series of hydraulic experiments was conducted in which the behavior of the water surface was altered by adjusting the general flow conditions of a range of uniform shallow flows over a sediment boundary. During these tests, the dynamics of the free surface boundary were measured carefully at a number of locations. The experiments were carried out in a 12 m long, sloping rectangular flume at the University of Bradford (see Figure 2(a)). The flume was 459 mm wide and it was set to a fixed slope of 0.004. The acoustic measurement section of the flume, and the section equipped with wave probes, were located at 8.4 m and 9.6 m from the upstream end of the flume, respectively. As shown in Figure 2(b), the flume bed was composed of a hexagonally packed arrangement of spheres of diameter $d_s = 25$ mm. The spheres in this work were manufactured by plastic injection moulding, and had a density of $\rho_s = 1400$ kg/m^3. Two layers of spheres were used in order to give a bed thickness of $h_b \approx 45$ mm which allowed interfacial flows into and out of the porous bed.

A constant head pump was used to recirculate water in the flume. Control of the discharge from the pump was achieved with an adjustable valve in the flume inlet pipe. The size of the discharge was determined using a u-tube manometer connected to a standard orifice plate assembly. The depth of the flow was controlled with an adjustable gate at the downstream end of the flume to ensure uniform flow conditions throughout a section as long as possible and in particular the measurement sections of the flume. The uniform flow depth was measured with a point gauge which was accurate to the nearest 0.5 mm, and by wave probes accurate to 0.01 mm. The hydraulic conditions studied in this work were designed to investigate the change in the water surface patterns as a function of the flow depth and velocity for a range of turbulent flow conditions typically found in gravel bed rivers. A summary of the hydraulic properties of these flow conditions is given in Table I. The uniform flow depth, D, and the depth-averaged mean flow velocity, U, in these conditions were changed from 50 mm to 100 mm, and from 0.23 m/s to 0.54 m/s, (from Condition 1 to Condition 6), respectively. Table I also provides a summary of the Reynolds numbers which correspond to these six flow conditions.
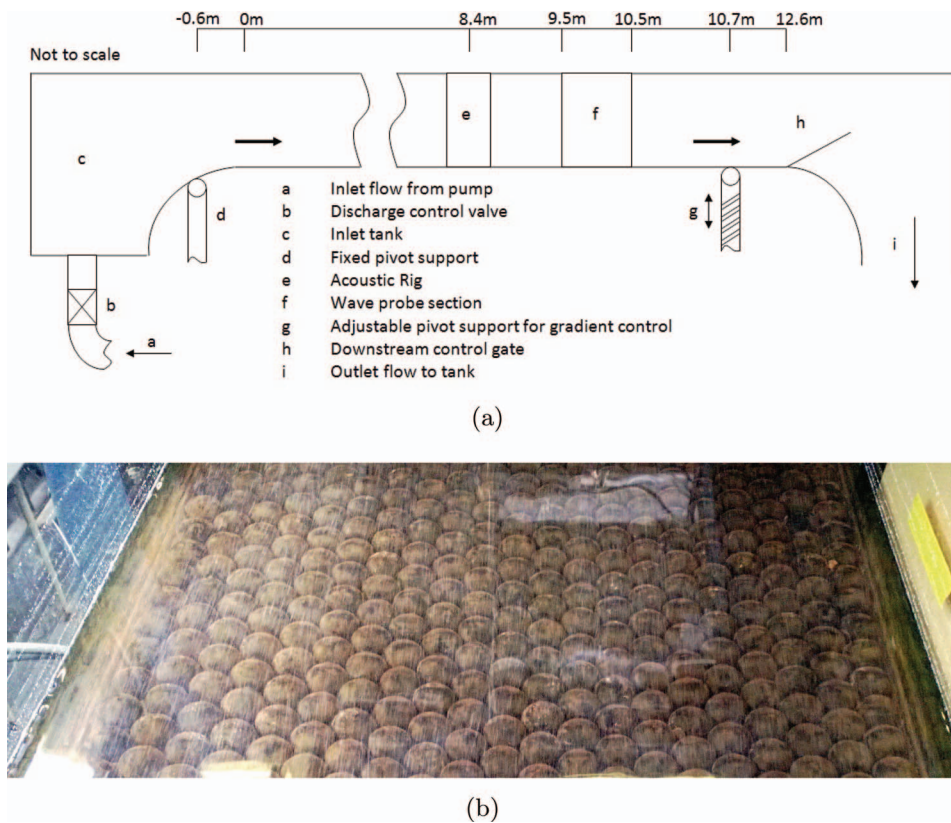
FIG. 2. Hydraulic flume: (a) diagram of flume with main dimensions; (b) hexagonal packing of spheres forming the flume bed.

The flow surface roughness characteristics were measured with a non-equidistant array of seven calibrated, conductance-based wave probes. This probe array was installed along the centreline of the flume to measure the instantaneous elevation of the water surface. Each of the probes in the array consisted of two vertical, parallel tinned copper wires which were separated by a 15 mm distance oriented laterally to the flow direction. The diameter of these wires was 0.24 mm. Figure 3 shows the position of the probe array with respect to the flume upstream end and indicates the streamwise separations between individual probes. The wave probes were regularly cleaned and calibrated to guarantee the accuracy of the wave height measurements for the adopted range of hydraulic conditions. The calibration procedure involved recording the voltage levels for all the probes under static, still

water conditions at six different water depths that spanned the full range of flow depths considered in this work (see Table I). This allowed linear regression lines to be empirically derived that allow the instantaneous voltage recorded on a particular probe to be converted into an accurate instantaneous water depth.

The probes were connected to standard WM1A wave probe control units provided by Churchill Controls. The outputs of the probe control units were connected through an analogue 10 Hz low-pass Butterworth filter to a National Instruments X-series PXIe-6356 data acquisition card. The control units provided an analogue output to the data acquisition card, which was capable of measuring to an accuracy of 2.5 mV. This was over an input range of -10 V to $+10$ V, which was tuned to cover depths from 0 mm to 200 mm, providing the potential to resolve the change in the water level of 0.025 mm. The accuracy of the wave probes was measured on still water that resulted in peak to peak variation $\pm$ 0.030 mm and root mean square error 0.015 mm.

It is worth mentioning the sources of errors which are associated with measuring the level of a dynamic free flow surface with wire wave probes. There are three basic effects which can influence the accuracy of a wire wave probe: (i) the formation of the meniscus on the wire; (ii) the generation of the flow run-up causing the apparent change in the flow level in the front and behind the wire; and (iii) the finite spacing between the wires in a wave probe. The first source of errors relates to the formation of a meniscus on each of the two wires in a wave probe. The maximum static height of the meniscus on a flat surface of the wire can be as high as $\delta h \simeq \sqrt{2} L_c$,

TABLE I. The characteristics of the 6 hydraulic conditions used for the experiments along with the surface roughness characteristics.

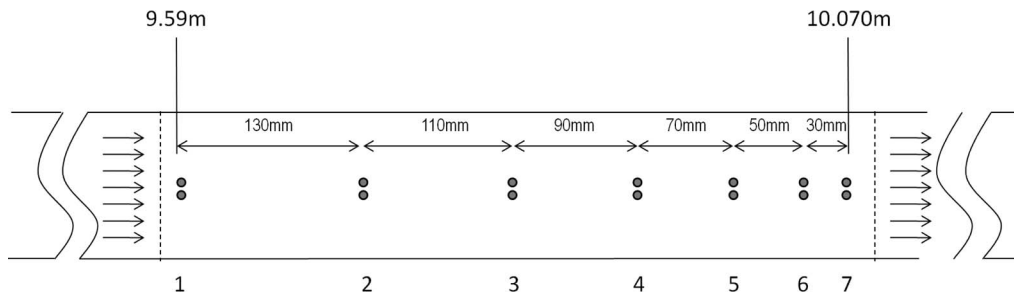| Flow condition	Depth, D, (mm)	Velocity, U, (m/s)	Re	Mean roughness height, σ, (mm)	Correlation radius, l, (mm)	Characteristic spatial period, L_0, (mm)
1	50	0.23	9823	0.29	110	100
2	60	0.31	17 436	0.45	140	100
3	70	0.37	24 450	0.56	170	143
4	80	0.44	29 713	0.65	230	175
5	90	0.51	36 852	0.67	250	203
6	100	0.54	45 675	0.84	270	224

FIG. 3. The orientation, position, and separations of the 7 wave probes in the test section of the flume.

where $L_c = 2.7$ mm is the capillary length for water-air interface at 25 °C.[14] In the case when the flow surface oscillates, this meniscus moves with the flow and in doing so its top contact points are likely to become smeared over the round wire cross-section resulting in some error in resistance measurement. It can be suggested that the maximum accuracy, this device can yield is a half of the wire diameter, which in this particular case equates to ±0.12 mm. The second source of errors relates to the formation of the run-up on the front of the wire, and depression at the rear as it is shown in the case of a vertical cylinder in a steady stream of water.[15] The surface resistance force acting on the wire is $F_s = 1/2 C_s \rho_w U^2 d^2$, where $\rho_w = 1000$ kg/m³ is the density of water, $d = 0.24$ mm is the diameter of the wire and C_s is the surface drag coefficient. It has been shown that the surface drag coefficient for a stretched wire of circular cross-section is less than 0.0471 for flows with the Froude number[15] Fr > 3. Because the Froude number for the flow conditions considered in this work is Fr > 4.7, it can be shown that the surface resistance force for the fastest flow condition (condition 6 with $U = 0.54$ m/s) is $F_s \simeq 4 \times 10^{-7}$ N. This force is sufficient to generate pressures which can cause the maximum displacement of a volume of fluid with dimension that is equivalent to the wire diameter, i.e., ±0.24 mm. The third source of errors is the discretization error related to the finite spacing between the two wires in the probe and it is discussed in detail in Sec. IV B.

The data acquisition card digitized the analogue wave probe signals simultaneously at 10 kHz in 1 ms packets. Each of these packets was acquired at a trigger rate of 100 Hz and the water level measured within each 1 ms packet was averaged to eliminate any chance of periodic high frequency noise. The resultant 300-s 100 Hz digitized wave probe signals were detrended. The mean roughness height was calculated from

$$\sigma = \frac{1}{7} \sum_{m=1}^{7} \sigma_m, \qquad (30)$$

where

$$\sigma_m = \sqrt{\frac{1}{T} \int_0^T \eta_m^2(t)\mathrm{d}t}, \qquad (31)$$

and $\eta_m(t)$ being time-dependent water surface elevation measured with the wave probe m over the period $T = 300$ s. The variability in the mean roughness heights for the seven wave probes for a given flow condition was less that 10%. The mean

roughness height values calculated from Eq. (30) for the six hydraulic conditions are listed in Table I.

The spatial correlation function was determined in two steps. Initially, the temporal, normalized cross-correlation function between wave probes m and n was estimated from

$$W_{mn}(t) = \frac{1}{T \sigma_m \sigma_n} \int_0^T \eta_m(\tau)\eta_n(t - \tau)\mathrm{d}\tau. \qquad (32)$$

The temporal, normalised cross-correlation function $W_{mn}(t)$ was then presented as a function of the spatial lag, $r_l = U \times t$, so that the extremum value (either a maximum or minimum) in the temporal cross-correlation function that corresponded to the maximum similarity in the water surface roughness pattern transported by the water flow from probe m to probe n within the analysis window could be determined. It has been shown[2] that the behavior of this function can be approximated by a simple analytical expression which combines the properties of an exponentially decaying function and a periodic process, e.g.,

$$W(\rho) = \mathrm{e}^{-\rho^2/l^2} \cos\left(\frac{2\pi}{L_0}\rho\right), \qquad (33)$$

where ρ is the spatial lag. The parameters l and L_0 in (33) relate to the correlation radius and characteristic period in the surface wave pattern, respectively. These two parameters were determined using the optimization procedure described in Ref. 2 and their values for the six hydraulic conditions are listed in Table I. These parameters were used to estimate the ratio l/L_0 and the error in the wave probe data from the knowledge of the spatial period (see Sec. IV).

B. Acoustic setup

The acoustic system was installed at the center of the flume and at 8.4 m from its upstream end. A semi-circular arch-shaped rig was constructed in order to precisely control the positioning of each of the acoustic components as shown in Figure 4. The arch was supported at each corner by a screw thread, allowing the height to be accurately adjusted. The base of the arch was thereby fixed at a distance of 10 mm above the mean water surface level for all flow conditions. The circumferential length of the arch was 1.26 m. A 40 mm diameter ultrasonic transducer (ceramic type 043SR750) was attached to the arch at a circumferential position of 945 mm and tilted downwards projecting downstream of the flow at 45° as shown in Figure 4. The distance between the center of
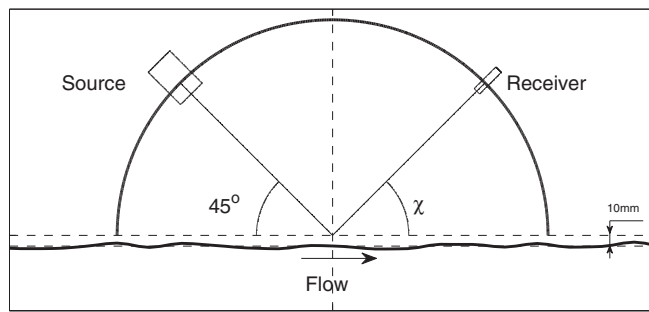
FIG. 4. The experimental setup for the acoustical measurements.

the transducer to the specular reflection point on the still water surface was 0.36 m. In this way, the specularly reflected wave was expected to arrive at the 315 mm position in the opposite part of the arch. Four 1/4-in. Bruel and Kjaer microphones of Type 4930 were initially placed at circumferential positions of 205, 305, 325, 425 mm, respectively, on the part of the arch opposite to the transducer. These four microphones were then moved in steps to cover uniquely a range of 40 angles from 16.43° to 73.57°, in increments of approximately 1.43°. The positions of the source and microphone array were then exchanged, so that the source was now projecting upstream of the flow. The same measurement procedure was repeated at the equivalent 40 positions on the opposite side of the arch for the same range of angles. The ultrasonic transducer was excited at its resonant frequency of 43 kHz with a 10 V sinusoidal signal generated by a Tektronix AFG 3021B function generator. The directivity of the transducer was measured in the free field and these data were used to predict the amplitude of the acoustic field projected on the surface of the still water as a function of the horizontal coordinate. The result of this prediction is shown in Figure 5. It enabled estimation of the streamwise characteristic length of the illuminated area of the water surface using the e^{-1} criteria which gives $L \approx 125$ mm, suggesting that the correlation radius $L < l$ is large for all the experimental regimes considered in this work.
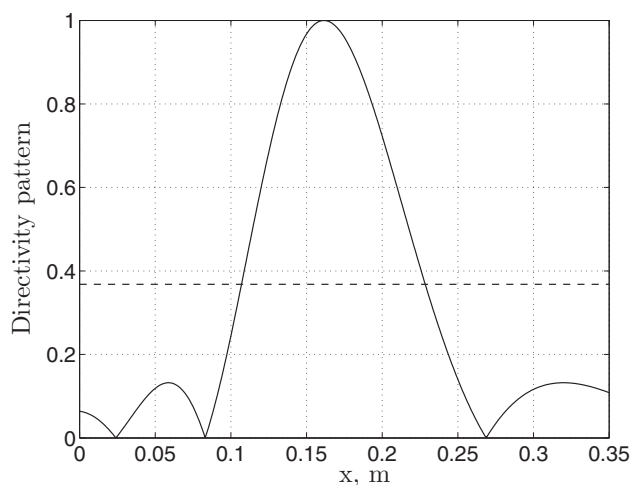

FIG. 5. The distribution of the acoustic pressure projected by the directional source on the surface of still water. The dashed line shows the e^{-1} threshold which was used to estimate the streamwise characteristic length of the illuminated area.
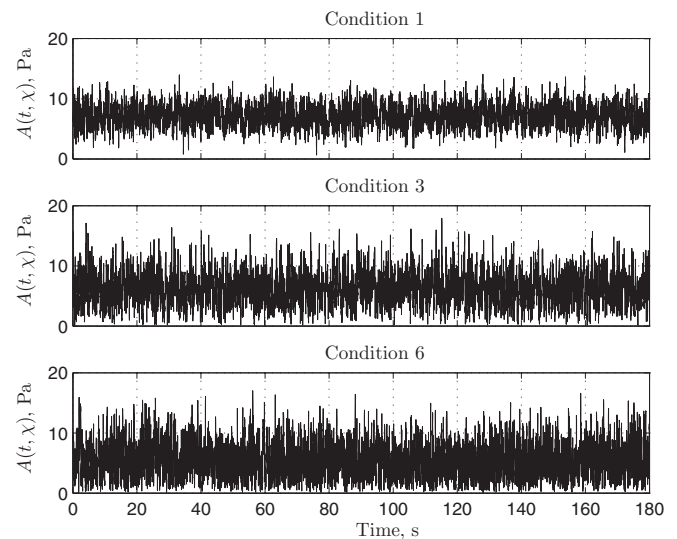

FIG. 6. Examples of the time histories of the amplitude of the acoustic signals recorded at $\chi = 45°$ for flow conditions 1, 3, and 6.

The microphone signals were conditioned using a Bruel and Kjaer Nexus 2690 four-channel microphone conditioning amplifier. The output sensitivity of the conditioning amplifier was set to 100 mV/Pa. A National Instruments NI PXIe-6356 data acquisition card was used to digitize the acoustic signals at 1 MHz sampling rate. The acquired data time series were 300 s long, so the data acquisition was carried out in 1 ms packets to avoid memory overflow. These packets of data were recorded for all 4 microphone and 7 wave probe channels and the acquisition of each packet was triggered at a rate of 100 Hz. The resulting raw data were saved into text files, so that analysis could be later performed.

The analysis of the recorded sound pressure signals was carried out in 1 ms packets. This analysis involved the calculation of the amplitude $A(t_j, \chi)$ of each 1 ms packet of acoustic pressure data recorded at the time instant, t_j, and at some angle along the arch, χ. Figure 6 shows an example of the time histories of the amplitude of the reflected sound wave which were recorded at the point of specular reflection (45° along the arch) for conditions 1, 3, and 6. The mean sound pressure as a function of angle was determined from these data according to the following expression:

$$P(\chi) = \frac{1}{J} \sum_{j=1}^{J} A(t_j, \chi). \tag{34}$$

C. The minimisation procedure

In this paper, the parameter inversion was based on the nonlinear least square minimisation technique.[16] This procedure was implemented in the commercial software MATLAB using the function lsqnonlin to determine the optimal values of the mean roughness height σ for which the discrepancy between the measured angular-dependent mean sound pressure and that predicted with the theory proposed in Sec. II A takes a minimum. In this procedure, the following objective
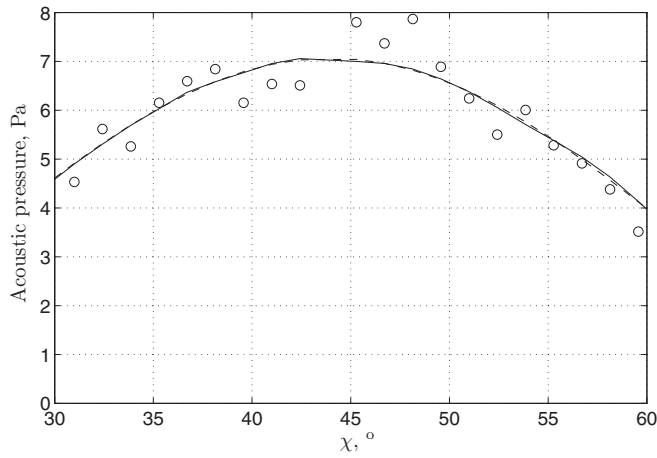
FIG. 7. The normalized amplitude of the reflected acoustic pressure over still water surface obtained with the Kirchhoff integral ("–") and stationary phase point approximation ("- -") and compared with data ("o").

function was formulated:

$$F(\sigma) = \sum_{j=1}^{N} [p_s(\chi_j, \sigma) - P(\chi_j)]^2, \qquad (35)$$

where N is the total number of angles for which the minimum of $F(\sigma)$ is sought, $p_s(\chi_j, \sigma)$ are the mean sound pressures predicted for these angles either by Eqs. (19) or (29) and $P(\chi_j)$ are mean sound pressures measured at these angles in either the up- or downstream direction. The prediction of $p_s(\chi_j, \sigma)$ requires the knowledge of the directivity amplitude $\mathcal{A}$ in Eq. (6). This parameter was determined from the same minimisation procedure (see Eq. (35)) in which the still water data for either down- or upstream direction were used and the value of the mean roughness height was set to $\sigma = 0$ in Eqs. (19) and (29). In this paper, the minimisation was performed in the vicinity of the specular reflection point of $\chi = 45° \pm 15°$. In this range, the directivity of the source was no more than 20 dB below the maximum. For this angular range, the number of data points used in the minimisation procedure was set to $N = 20$.

Figure 7 shows the theoretical predictions for the mean sound pressure which were obtained by using Eqs. (19) and (29) for the case of the smooth (still) water with $\sigma = 0$. This figure also presents the measured data. It is observed that for the angular interval $\chi = 45° \pm 15°$ accuracy of the prediction obtained with the input parameters mentioned in Sec. III is within 5% of the data.

IV. THE RESULTS

A. The deduced mean roughness height data

Figures 8(a)–8(f) show the results of inversion which were obtained through the application of the minimisation procedure given by Eq. (35). These results show that the mean sound pressure calculated in accordance with Eq. (29) agrees with that calculated via the Kirchhoff integral to within 1% in a relatively wide angular interval of $30° < \chi < 60°$. The agreement between these predictions and data is within 5% in the angular interval of $\chi = 45° \pm 15°$ for all the flow con-

ditions considered in this work. Table II presents the values of the mean roughness height which were deduced through the minimisation of the differences between the data and predictions by the Kirchhoff integral (σ_K) and minimising the difference between the data and predictions by the stationary phase method (σ_{sp}). It is reported that the difference between two methods is within 5%. Table II also shows the value of the mean roughness height measured with the wave probes. The maximum relative error between the measured and deduced standard deviation is 55%, which occurred in the case of flow condition 2.

A good agreement between the stationary phase point approximation and integral solution shows that the directivity of the scattered sound pressure depends strongly on the mean roughness height and in the same way as suggested in Ref. 17 for the case of the Fraunhofer zone. Therefore, at every point of angular pattern the reflection will be reduced by the order of $\exp(-\sigma^2 q_z^2/2)$. Using Eq. (29), one can find explicitly standard deviation in terms of the normalized data as

$$\sigma'_{sp} = \frac{1}{q_z(\chi)}\sqrt{2\ln\left(\frac{p_s(\sigma = 0, \chi)}{P(\chi)}\right)}, \qquad (36)$$

where $p_s(\chi)$ is derived with Eq. (29) for $\sigma = 0$ and $P(\chi)$ is given by Eq. (34). Equation (36) depends on the receiver angle χ. In Table II, the values quoted for the mean roughness height derived with Eq. (36) are averaged within the angular interval of $\chi = 45° \pm 15$. The results are accurate within 5% from those obtained with minimization technique.

Equation (36) shows that small errors in the value of $p_s(\sigma = 0, \chi)$ which can be caused by the change in the source amplitude, $\mathcal{A}$, are amplified because of the log function in Eq. (36) and contribute significantly to the error in the predicted mean roughness height of the surface. It can be seen from Figure 9 that variation of 5% in amplitude can cause more than 20% decrease/increase in the mean roughness height recovered with this acoustical method. This effect is similar to that encountered in the remote sensing techniques and it is related to ill-posed problems (see Ref. 18) so that care should be taken while estimating the source amplitude, $\mathcal{A}$ and related angular spectrum of $p_s(\sigma = 0, \chi)$.

Figure 10 compares graphically the values of the mean roughness height data measured with the wave probes and deduced using the acoustical method. This figure also shows the regression line $\sigma_K = \mathcal{C}\sigma$ with regression coefficient $\mathcal{C} = 0.77$ obtained to fit σ_K and with the coefficient of determination $\mathcal{R}^2 = 0.86$. A straightforward substitution of σ_{sp} or σ'_{sp} for σ_K in the regression analysis does not change the value of $\mathcal{C}$ by more than $\pm 1.5\%$. This suggests that the acoustical method can be calibrated and used to deduce the mean roughness height with the relative error of 5% for the hydraulic conditions studied in this work. This acoustic instrumentation is particularly attractive to use in the case when the ratio σ/L_0 becomes large. In this case, the accuracy of the wave probes reduces because of the increased discretisation error caused by the finite value of the spacing between the wires in the probe, or *in situ* when the use of the wave probes is impractical.
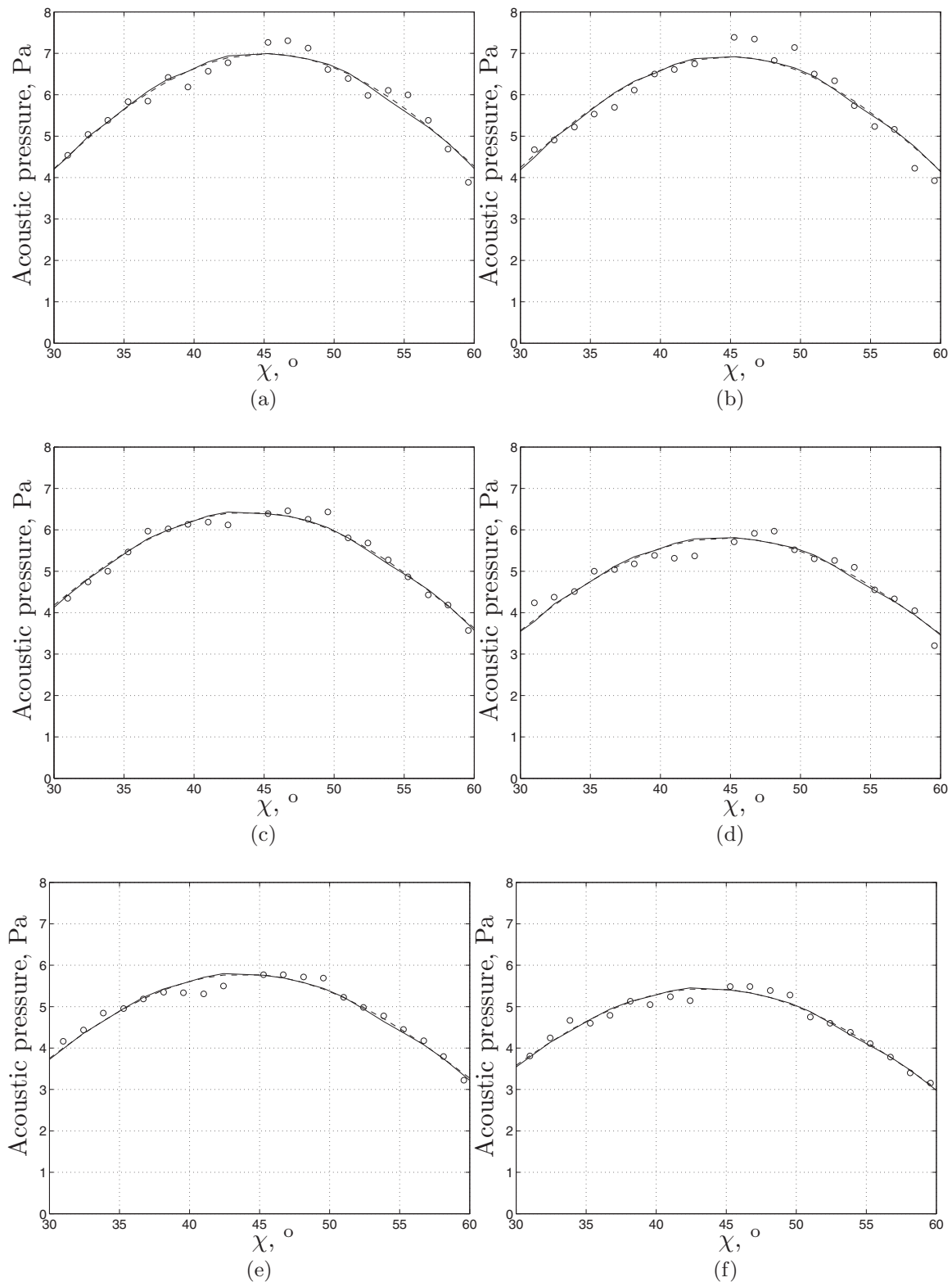
FIG. 8. The normalized amplitude of scattered acoustic pressure over rough surface generated by the water flow with the depth: (a) 50 mm, (b) 60 mm, (c) 70 mm, (d) 80 mm, (e) 90 mm, (f) 100 mm. Data ("o") are compared against predictions based on the Kirchhoff integral ("–") and stationary phase point approximation ("- -").

B. The discretization error in wire wave probe measurements

The problem of the discretization error in the case of wire wave probe measurement is easy to illustrate when the sur-

face roughness pattern can be approximated as $\eta(r) \sim \sigma e^{iK_0 r}$, where $K_0 = 2\pi/L_0$ is the characteristic wavenumber in the surface roughness. In this case, the wave probe resistance is the mean between the two instantaneous water level elevations, $\eta(r_1)$ and $\eta(r_2)$, at the positions of the two wires spaced by the

TABLE II. The values of the mean roughness height derived through the Kirchhoff integral (σ_K), stationary phase point approximation (σ_{sp}) and as an average for Eq. (36). The directly measured values of the mean roughness height (σ) are also quoted to enable a comparison.

Flow condition	Flow depth, mm	σ_K, mm	σ_{sp}, mm	σ'_{sp}, mm	σ, mm
1	50	0.15	0.15	0.14	0.29
2	60	0.2	0.19	0.21	0.45
3	70	0.41	0.4	0.4	0.56
4	80	0.57	0.57	0.56	0.65
5	90	0.58	0.57	0.57	0.67
6	100	0.66	0.66	0.65	0.84

distance $\Delta r = r_2 - r_1$. The instantaneous water level measured with this wave probe is $\hat{\eta}(r_1) \sim \sigma e^{iK r_1}\left(1 + e^{iK\Delta r}\right)/2$, which will underestimate the true water level at the position r_1 by the term $|(1 + e^{iK\Delta r})/2|$. It is of interest to estimate this term for the hydraulic regimes studied in our work. The value of this term depends on the characteristic spatial period of the roughness (L_0) and wire spacing (Δr). In the streamwise direction, the characteristic spatial period ($100 \leq L_0 \leq 224$ mm). However, the separation between the wires in the wave probes is in the lateral direction. The work by Roy *et al.*[19] suggests that the lateral dimension of the turbulent flow structures is 0.5–1.0 of the flow depth which was $50 \leq D \leq 100$ mm. Therefore, we can assume that the characteristic spatial period of the turbulence-generated surface roughness in the lateral dimension is comparable to that in the streamwise direction and we consider the range of $50 \leq L_0 \leq 224$ mm. The lower value here is taken as the minimum depth of the water flow which, according to the work by Roy *et al.*[19]) can be taken as a lateral dimension of the turbulent structures causing this roughness to occur.

It is necessary to know the spatial spectrum of the roughness pattern in order to estimate the actual error in the wave probe readings caused by the finite value of Δr. This power
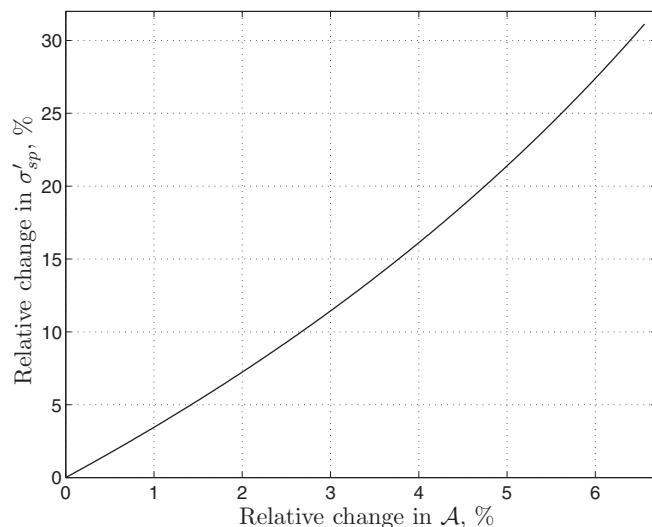

FIG. 9. The variation in the deduced mean roughness σ'_{sp} as a function of the relative change in the source amplitude, $\mathcal{A}$.
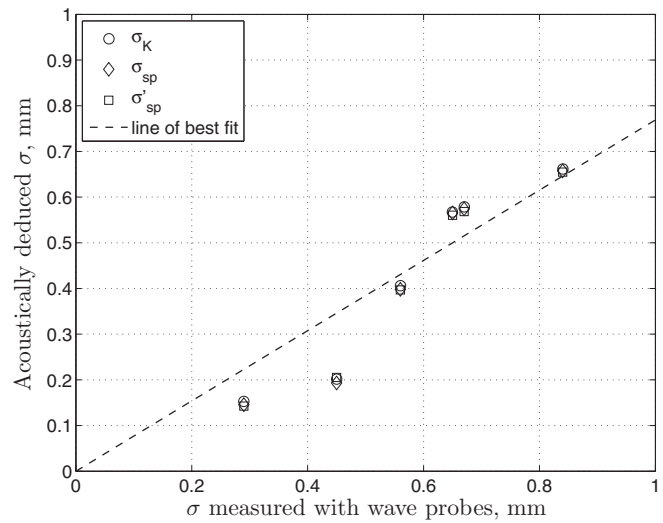

FIG. 10. The correlation between the mean roughness height measured with the wave probe array and mean roughness height deduced with the proposed acoustical method.

spectrum can be estimated for a given hydraulic regime through the knowledge of the spatial correlation function (Eq. (33)) and Wiener-Kinchin theorem, i.e.,

$$\tilde{W}(K) = \int_{-\infty}^{+\infty} W(\rho)e^{-iK\rho}\,d\rho. \tag{37}$$

The application of the Fourier transform results in a simple analytical expression

$$\tilde{W}(K) = \frac{1}{2}[\tilde{G}(K - K_0) + \tilde{G}(K + K_0)], \tag{38}$$

where

$$\tilde{G}(s) = \int_{-\infty}^{+\infty} e^{-\rho^2/l^2}e^{-is\rho}\,d\rho = \sqrt{\pi}l e^{-l^2 s^2/4}. \tag{39}$$

The above arguments enable us to suggest that the relative measurement error due to the finite distance between the wave probes can be expressed as the following:

$$e\left(K_0\right) = \left(1 - \sqrt{\frac{\hat{v}}{v}}\right) \times 100\%, \tag{40}$$

where

$$\hat{v} = \sigma^2 \frac{\sqrt{\pi}l}{2\pi} \int_{-\infty}^{+\infty} \frac{1}{8}|1 + e^{iK\Delta r}|^2$$
$$\times [e^{-l^2(K-K_0)^2/4} + e^{-l^2(K+K_0)^2/4}]dK$$
$$= \frac{\sigma^2}{2}[e^{-\Delta r^2/l^2}\cos(K_0\Delta r) + 1] \tag{41}$$

and

$$v = \sigma^2 \frac{\sqrt{\pi}l}{2\pi} \int_{-\infty}^{+\infty} \frac{1}{2}[e^{-l^2(K-K_0)^2/4} + e^{-l^2(K+K_0)^2/4}]dK = \sigma^2 \tag{42}$$

are the variance in the roughness height estimated with the wave probe and variance of the actual height, respectively.

Equation (40) enables us to estimate the error in the wave probe measurements due to the finite value of $\Delta r = 15$ mm for a range of flow regimes. The largest error occurs when

the value of the characteristic period is the shortest. If we assume that that the minimum characteristic spatial period in the lateral direction $L_0 = 50$ mm and $l \approx 1.4 L_0$ (which is true for all the hydraulic regimes considered in this work, see Table I), then the relative error given by Eq. (40) is 41%. This error is 11% for flow condition 1 ($L_0 = 100$ mm and $l = 110$ mm), 6% for flow condition 3 ($L_0 = 143$ mm and $l = 170$ mm) and 2% for flow condition 6 ($L_0 = 224$ mm and $l = 270$ mm). The values of these errors are comparable with the differences between the values of the mean roughness height deduced with the acoustical method and measured with the wave probe array. The data shown in Table II suggest that the relative difference between the acoustically deduced roughness and that measured with the wave probes is below 15% for flow conditions 4 and 5 for which the ratios $\Delta r/L_0$ and $k\sigma^2/R$ remain much smaller than 1. This difference increases to 20% for flow condition 6 which can be explained by the fact that the condition for the Fraunhofer zone, $k\sigma^2/R \ll 1$ is no longer satisfied.

C. The relationship with the hydraulic parameters

The deduction of mean roughness height without submerging any instrumentation in water carries significant importance and offers the opportunity to estimate some of the hydraulic properties of a given open channel flow based on the non-invasive acoustic measurements with a stationary source and several stationary receiver points or with a roaming receiver as described in this paper. The vertical scale of free surface features is inherently linked to the degree of kinetic energy within the flow, resulting in a clear dependence between mean roughness height and mean flow velocity as proved previously with data presented in Chap. 5 of Ref. 3 and in Table I in Ref. 2. Figure 11 shows a clear relationship between the normalised mean water surface roughness height and the depth-based flow Reynolds number for all the flow conditions examined in this work. This relationship follows closely a linear dependence for the range of flow conditions considered in
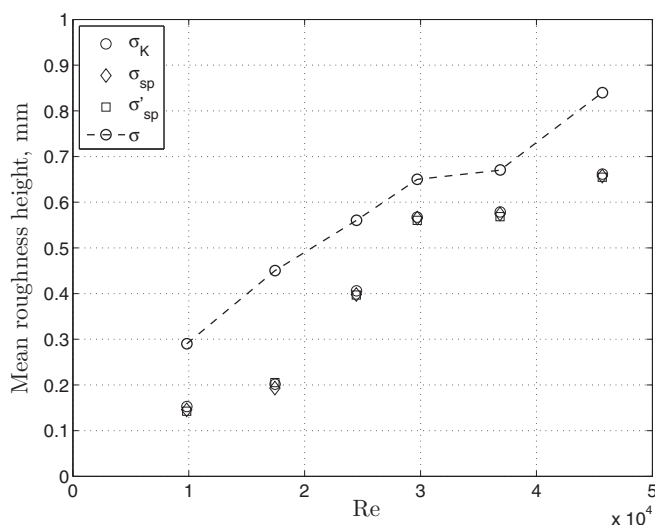
FIG. 11. The mean roughness height plotted as a function of the Reynolds number.

this work. The acoustical method which is able to estimate the flow Reynolds number within a 5% accuracy, provided the acoustic setup is calibrated. This technique is more simple than others such as acoustic phase tracking[20] or Doppler backscattering technique[21] which requires more sophisticated data analysis.

Further to the velocity and Reynolds number measurements, it has also been shown that the mean roughness height carries information regarding the longitudinal length scales of turbulent structures beneath the flow surface.[3] This is thought to be due to larger turbulent structures exhibiting a greater propensity to deform the free surface. In this manner, a remote acoustical method for determining mean roughness height can facilitate the deduction of the length scales of dominant turbulent processes within the flow. This information is critical for understanding the mixing properties of turbulent flows, for example, when assessing the behavior and impact of pollutant and sediment transport. The properties of turbulent processes within shallow flows are inherently linked to the bed roughness shape, so that a non-invasive measurement of these properties can facilitate the estimation of the hydraulic roughness coefficient,[2] a quantity important for predicting the flow capacity of rivers and man-made infrastructure and its potential to cause flooding. Higher flow depths generally allow the formation of larger scale turbulent structures (see Chap. 5 in Ref. 3), and therefore larger surface roughness.

V. CONCLUSIONS

In this paper, the airborne acoustic waves generated by the source with directivity pattern of a piston in the rigid baffle are applied to study the statistics of the rough surface of shallow water flow in open channels. It is shown that a straightforward inversion technique based on the single stationary phase point approximation can be used to deduced the mean roughness height of the surface of a turbulent flow. Either the non-linear curve fitting method (35) or explicit formulation (36) can be used for this inversion process. The proposed techniques have been tested for several flow conditions and the results of inversion have been compared with the data obtained with conductance-based wave probes. It is concluded that the mean roughness height can be estimated acoustically with a $\pm 5\%$ error, provided the acoustic setup is calibrated and the $\chi = \chi_0 \pm 15°$ (χ_0 being the angle of specular reflection) range of angles is adopted for the inversion. It is also shown for the given flow conditions that the roughness mean hight can be used to estimate the Reynolds number and uniform flow depth.

The ability to measure the mean roughness height without submerging any instrumentation in water carries significant importance. This method offers the opportunity to estimate the Reynolds number and flow velocity in a given open channel flow using a stationary sound source and several receiver points arranged in the forward scattering direction. It allows for non-invasive monitoring of shallow flows in environments ranging from natural rivers to urban drainage systems and offers an opportunity for low-cost and low-maintenance monitoring of hydraulic flows on a very large scale, thus enabling proactive maintenance and better

resilience against asset degradation, blockage formation, and flooding.

[1]S. Kumar, R. Gupta, and S. Banerjee, Phys. Fluids **10**, 437 (1998).

[2]K. V. Horoshenkov, A. Nichols, S. J. Tait, and G. A. Maximov, J. Geophys. Res.–Earth **118**, 1864, doi:10.1002/jgrf.20117 (2013).

[3]A. Nichols, Ph.D. thesis, University of Bradford, 2014.

[4]K. V. Horoshenkov and A. Nichols, "Methods and apparatus for detection of fluid interface fluctuations," U.S. patent application 14,002,569 (19 December 2013).

[5]S. P. Walstead and G. B. Deane, J. Acoust. Soc. Am. **133**, 2597 (2013).

[6]F. G. Bass and I. M. Fuks, *Wave Scattering from Statistically Rough Surfaces* (Pergamon, Oxford, 1979), p. 186.

[7]R. D. Kodis, IEEE T. Antenn. Propag. **14**, 77 (1966).

[8]M. S. Longuet-Higgins, J. Opt. Soc. Am. **50**, 845 (1960).

[9]M. S. Longuet-Higgins, J. Opt. Soc. Am. **50**, 851 (1960).

[10]S. M. Rytov, Yu. A. Kravtsov, and V. I. Tatarskii, *Principles of Statistical Radiophysics 1: Elements of Random Process Theory* (Springer-Verlag, New York, 1987), p. 108.

[11]P. M. Morse and K. Uno Ingard, *Theoretical Acoustics* (McGraw-Hill, New York, 1968), p. 381.

[12]M. V. Fedoryuk, Comput. Math. Math. Phys. **2**, 145 (1963).

[13]D. E. Barrick, IEEE T. Antenn. Propag. **16**, 449 (1968).

[14]B. Lautrup, *Physics of Continuous Matter, Second Edition: Exotic and Everyday Phenomena in the Macroscopic World* (CRC Press, Boca Raton, 2011), p. 81.

[15]J. R. Chaplina and P. Teigen, J. Fluid. Struct. **18**, 271 (2003).

[16]See http://www.mathworks.co.uk/help/optim/ug/lsqnonlin.html for optimization algorithm; assessed on 19 March 2014.

[17]M. A. Isakovich, J. Exp. Theor. Phys. **23**, 305 (1952) (in Russian).

[18]A. Ishimaru, *Wave Propagation and Scattering in Random Media* (Academic Press, New York, 1978), p. 504.

[19]A. G. Roy, T. Buffin-Belanger, H. Lamarre, and A. Kirkbride, J. Fluid Mech. **500**, 1 (2004).

[20]A. Nichols, S. Tait, K. Horoshenkov, and S. Shepherd, Flow Meas. Instrum. **34**, 118 (2013).

[21]L. B. Marsh and D. B. Heckman, "Open channel flowmeter utilizing surface velocity and lookdown level devices," U.S. patent 5,811,688 (22 September 1998).